

PAPER • OPEN ACCESS

Experimental characterization of the active and passive fast-ion H-alpha emission in W7-X using FIDASIM







To cite this article: Peter Zs. Poloskei *et al* 2024 *Nucl. Fusion* **64** 026008

View the [article online](#) for updates and enhancements.

You may also like

- [Dual view FIDA measurements on MAST](#)
C A Michael, N Conway, B Crowley et al.
- [On velocity-space sensitivity of fast-ion D-alpha spectroscopy](#)
M Salewski, B Geiger, D Moseev et al.
- [Fast-ion D alpha diagnostic with 3D-supporting FIDASIM in the Large Helical Device](#)
Y. Fujiwara, S. Kamio, H. Yamaguchi et al.

Experimental characterization of the active and passive fast-ion H-alpha emission in W7-X using FIDASIM

Peter Zs. Poloskei^{1,*} , B. Geiger² , A. Jansen van Vuuren^{3,6} , S. Äkäslompolo^{1,4} , O.P. Ford¹ , A. Spanier¹, T.W.C. Neelis⁵, P. McNeely¹, D. Hartmann¹  and the W7-X Team^a

¹ Max-Planck Institute for Plasma Physics, 17489 Greifswald, Germany

² University of Wisconsin-Madison, Madison, WI, United States of America

³ University of Seville, Seville, Spain

⁴ Aalto University, Espoo, Finland

⁵ Eindhoven University of Technology, 5612 AZ Eindhoven, Netherlands

⁶ Max-Planck-Institut für Plasmaphysik, 85748 Garching, Germany

E-mail: peter.zsolt.poloskei@ipp.mpg.de

Received 17 July 2023, revised 13 September 2023

Accepted for publication 17 November 2023

Published 22 December 2023



Abstract

This paper presents the first results from the analysis of Balmer-alpha spectra at Wendelstein 7-X which contain the broad charge exchange emission from fast-ions. The measured spectra are compared to synthetic spectra predicted by the FIDASIM code, which has been supplied with the 3D magnetic fields from VMEC, 5D fast-ion distribution functions from ASCOT, and a realistic Neutral Beam Injection geometry including beam particle blocking elements. Detailed modeling of the beam emission shows excellent agreement between measured beam emission spectra and predictions. In contrast, modeling of beam halo radiation and Fast-Ion H-Alpha signals (FIDA) is more challenging due to strong passive contributions. While about 50% of the halo radiation can be attributed to passive signals from edge neutrals, the FIDA emission—in particular for an edge-localized line of sights—is dominated by passive emission. This is in part explained by high neutral densities in the plasma edge and in part by edge-born fast-ion populations as demonstrated by detailed modeling of the edge fast-ion distribution.

Keywords: plasma physics, stellarator, forward modelling, fast-particle diagnostic

(Some figures may appear in colour only in the online journal)

^a See Sunn Pedersen *et al* 2022 (<https://doi.org/10.1088/1741-4326/ac2cf5>) for the W7-X Team.

* Author to whom any correspondence should be addressed.



Original Content from this work may be used under the terms of the [Creative Commons Attribution 4.0 licence](https://creativecommons.org/licenses/by/4.0/). Any further distribution of this work must maintain attribution to the author(s) and the title of the work, journal citation and DOI.

1. Introduction

Balmer-alpha spectroscopy allows versatile investigations of hydrogen plasmas [1–5]. In particular active spectroscopy with lines of sight intersecting the paths of neutral beams has become an important diagnostic technique since it carries localized information on important plasma parameters such as the fast-ion density, the radial electric field, plasma rotation, and the main-ion temperature. However, the complex shape of the measured spectra requires well-developed models for its interpretation [6, 7]. The Balmer-alpha emission at 656.281 nm is formed by the $n = 3 \rightarrow 2$ transition of excited hydrogen particles and is in the visible spectrum. For its detailed understanding often forward modeling is utilized. Fast-Ion D-Alpha SIMulation code (FIDASIM) [7, 8] is such a modeling tool, which was developed to predict the active Balmer-alpha spectrum and neutral particle analyzer signals [7] for tokamaks, assuming axi-symmetry. It has been used extensively on tokamaks such as AUG, DIII-D or TCV [9–13], but is novel to the world of stellarators [14].

Wendelstein 7-X [15] (W7-X) is a new stellarator, which was recently upgraded with two Neutral Beam Injection (NBI) sources [16–18] and active Balmer-alpha spectroscopy, installed as a subsystem of the Charge-Exchange Recombination Spectroscopy (CXRS) system [19]. It was possible to characterize parameters of the beam injection system, infer information on the main-plasma species temperature and rotation, and explore FIDA⁷ emission, which provides an important insight into the fast-ion population.

The paper is structured as follows: first, we discuss the extension of the code FIDASIM into the full 3D geometry of W7-X. After this, we introduce the spectroscopy system available at W7-X for Balmer alpha spectroscopy studies. Next, we present the details of the modeling and compare the measured and modeled beam emission, halo emission, and fast-ion Balmer alpha, FIDA emission. Finally, we conclude with a summary and outlook.

2. Extension of FIDASIM to full 3D for W7-X

FIDASIM follows neutral super-particle markers and solves rate equations to predict the neutral density from the $n = 1$ to $n = 6$ principal quantum states based on the local equilibrium plasma profiles. To map these quantities to a given spatial location, the 3D magnetic equilibrium reconstruction from variational moments equilibrium code (VMEC) [20] is used, which provides $\rho(R, Z, \phi)$ flux surface coordinates and the local magnetic field $\vec{B}(R, Z, \phi)$. An example of magnetic equilibrium can be seen in figure 1, (a) in a poloidal cross-section and (b) in a top-down view on the midplane. In addition, figure 1 shows the two NBI sources of W7-X operated during the 2018 experimental campaign in red and blue. Both sources

provide a nearly radial injection of fast neutral particles. A fast-ion distribution function, as calculated by the accelerated simulation of charged particle orbits in Tori (ASCOT) [21] code for the later investigated plasma discharge, is shown in figure 2. Pitch values (v_{\parallel}/v) close to 0.5 and -0.5 are being populated and the fast-ion density peaks in the plasma core region. FIDASIM has been upgraded to utilize the full 5D ($R, Z, \phi, E, v_{\parallel}/v$) fast-ion distribution function from ASCOT to predict synthetic spectra.

In addition to the fast-ion distribution function, FIDASIM requires information on the kinetic plasma profiles. At W7-X Thomson-scattering measurements are used for electron temperature and density and charge-exchange spectroscopy on carbon is used for the ion temperature as input to FIDASIM. The main impurity is assumed to be carbon, while the plasma rotation is neglected. A typical spectrum from FIDASIM can be seen in figure 3.

3. The charge-exchange spectroscopy system at W7-X

A highly flexible and extensive CXRS diagnostic was set up at W7-X [19] to provide high-resolution local measurements of different plasma parameters such as ion temperature, impurity density and to monitor beam attenuation and power deposition of the recently commissioned neutral beam heating system. The observation system consists of three different ports, looking from different angles at the plasma. The line-of-sight geometries are shown in 3D in figure 4. A21 is a toroidal view with roughly 0° inclination to the magnetic field at the beam intersection, while M21 and T21 are 45° views. The toroidal lines of sight and the T21 port views observe red-shifted beam emission while M21 port views observe the beam emission at blue-shifted wavelengths.

The measurements discussed here were made with an ITER Prototype Spectrometer (ILS) which allows the simultaneous measurement of spectra from 54 channels at three distinct wavelength ranges. One of the ranges is between 648–666 nm, which covers the Balmer-alpha emission line with 0.0125 nm spectral resolution. The measurement is absolute intensity calibrated, thus it provides measurement in units of (Photons $\text{sr}^{-1} \text{nm}^{-1} \text{m}^{-2} \text{s}^{-1}$).

Fast-ion Balmer-alpha emission can be locally interpreted as a weighted integral of the fast-ion distribution function with the observation's weight-function [22]. Weight functions characterize the observation's sensitivity to different parts of the fast-ion phase-space. They look similar for lines of sight from the same port as they are characteristic of the observation direction. One can be seen in figure 4(b) for each of the observation directions examined in this work.

4. NBI parameters as implemented in FIDASIM

During this work, W7-X was equipped with 2 NBI sources (referred to S7 and S8), with almost radial injection (see

⁷ Fast-ion Balmer-alpha is being abbreviated FIDA following the convention adapted from [7].

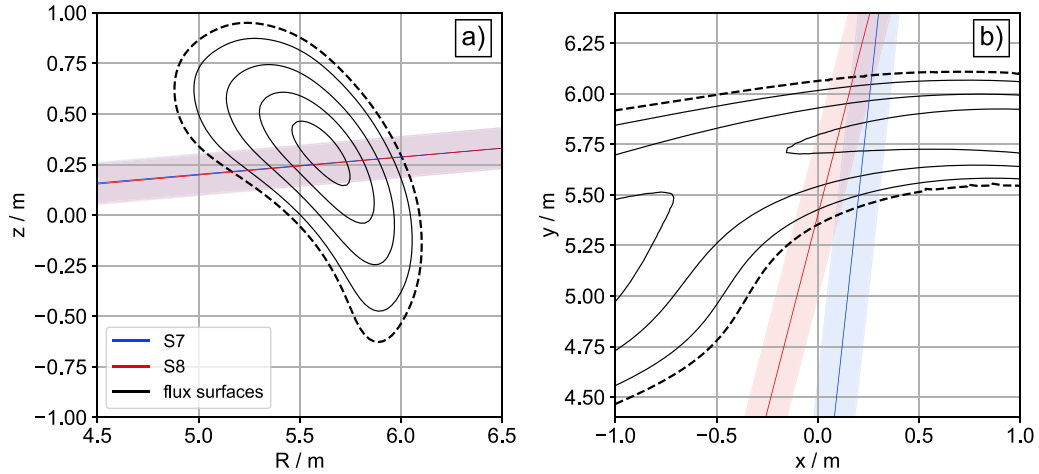


Figure 1. Equilibrium flux surfaces for W7-X (a) at $\phi = 88^\circ$ poloidal cross-section, (b) horizontal cross-section at the midplane. Flux surfaces marked with black line. The operated NBI sources (S7, S8) are marked with red and blue, shaded area indicating their designed effective width.

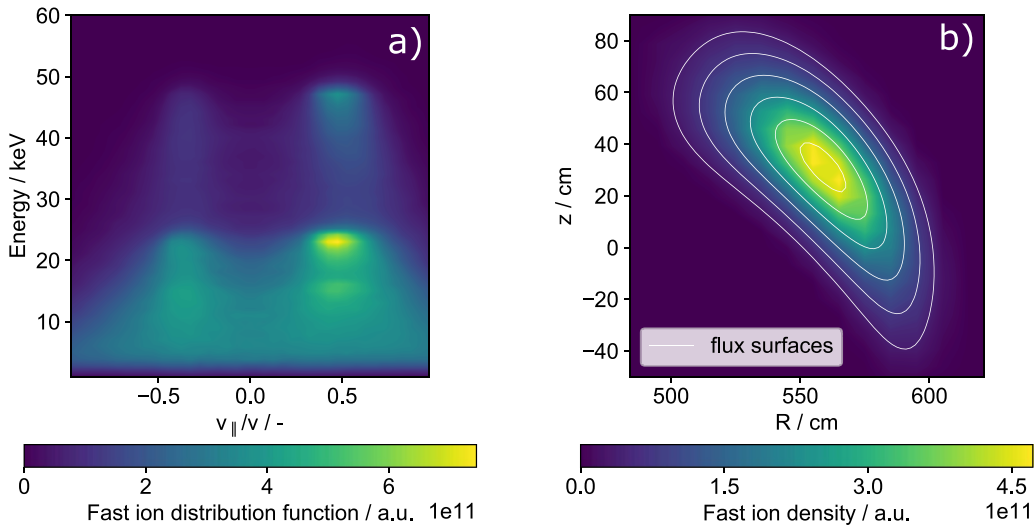


Figure 2. (a) Fast-ion distribution function in the beam-injection plane, averaged over the injection poloidal cross-section, and (b) the fast-ion density as predicted by ASCOT.

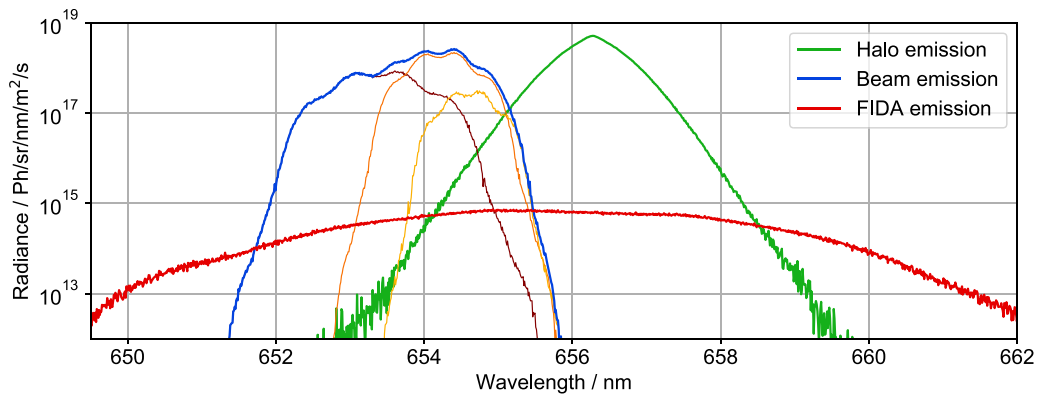


Figure 3. Typical Balmer-alpha spectrum predicted by FIDASIM for one of the observation lines of sight in discharge 20 180 823.037 at 5.2 s. Different colors mark different spectral components. Brown, orange and yellow colors are marking the different energy components of the beam emission. With green the unshifted halo emission and with red the broad FIDA emission is shown.

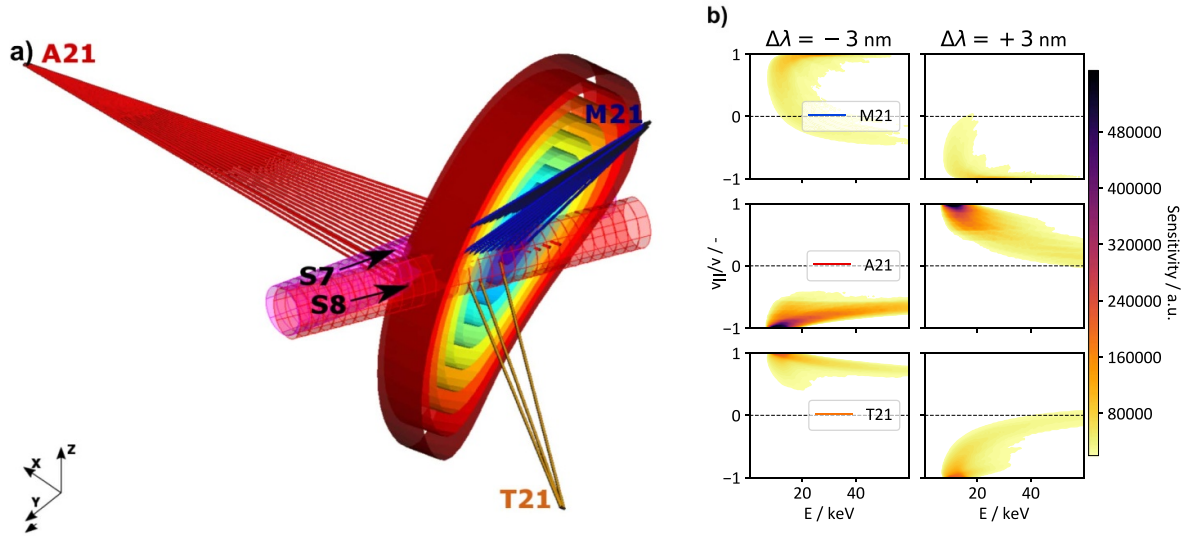


Figure 4. (a) Lines of sight 3D geometry of the three different observation systems, looking at two NBI sources S7 and S8: red A21 toroidal- and the orange T21 and blue M21 45°. (b) FIDA weight-functions calculated for one line of sight for each port to characterize the observation directions' sensitivity to the fast-ion phase-space.

Table 1. Position and direction vectors of sources S7 and S8 in Cartesian coordinates, as used in FIDASIM.

	x (cm)	y (cm)	z (cm)	u_x	u_y	u_z
S7	104.27	1317.11	90.67	-0.1085	-0.990	-0.085
S8	195.96	1300.37	90.67	-0.2486	-0.9648	-0.085

Table 2. Beamline parameters of sources S7 and S8, as used in FIDASIM. FIDASIM differentiates between horizontal and vertical parameters (with respect to the specific injection line's direction). D —size of the ion-source, where NBI markers are initialized; δ —beamlet divergence; f —focal length; L —distance of the first- and second aperture (beam blocking element) from the source; Δ —offset of the apertures' middle from the beam line; d —physical size of the apertures.

		D (cm)	δ (°)	f (cm)	$L_{1,2}$ (cm)	$\Delta_{1,2}$ (cm)	$d_{1,2}$ (cm)
S7	horizontal	22.8	0.8	650.0	626.9/708.4	1.7/1.9	34.1/34.1
	vertical	50.6	0.8	700.0	626.9/708.4	-4.8/3.2	67.0/57.4
S8	horizontal	22.8	0.8	650.0	626.9/708.4	5.6/-5.9	34.1/34.1
	vertical	50.6	0.8	700.0	626.9/708.4	-4.8/3.2	67.0/57.4

figure 1), operated with hydrogen. The nominal acceleration voltage is 55 keV with 0.3/0.6/0.1—full/half/third energy component density fractions. These parameters are measured by a spectrometer with a line of sight viewing the beamline inside the beam neutralizer [21]. S7 and S8 have a double purpose, both providing the source of fast-ions and neutrals for the CXRS measurements. The physical coordinates of the sources and their direction vector are listed in table 1 and originate from the design drawings.

To model NBI operation in FIDASIM, neutral markers are randomly initialized at the ion-source location. Given the horizontal and vertical focal points, a direction vector is assigned and randomly altered using the δ beamlet divergence. If the particle trajectory does not intersect the aperture provided opening (see figure 5 red arrow), a new marker is initialized, providing a fixed amount of NBI power to the plasma.

Tables 1 and 2 contains the beamline parameters used in FIDASIM.

5. Validation of FIDASIM based on beam- and halo-emission modelling

To validate FIDASIM, the predicted beam- and halo emission has been compared to the absolutely intensity calibrated measurements. Moreover, the predicted injected power has been compared with beam power calorimetry measurements [16]. For this purpose, a discharge #20180823.037, with both NBI sources operational was selected. This discharge was run in the 'high-mirror' [23] iota configuration, with 5 MW of continuous ECRH heating. Both NBI sources were turned on at 4.5 s and were operated for 1 s continuously. The beam injection power was 1.35 MW per source and the acceleration voltage was 48 keV with neutral particle flux fractions of 0.32/0.61/0.07 (full/half/third) identical for both sources. The core plasma temperature was 2.5 keV for electrons and 1.5 keV for ions, with a core-plasma electron density of $6.2 \cdot 10^{19} \text{ m}^{-3}$. Measured kinetic profiles can be seen in figure 6 at 4.5 s.

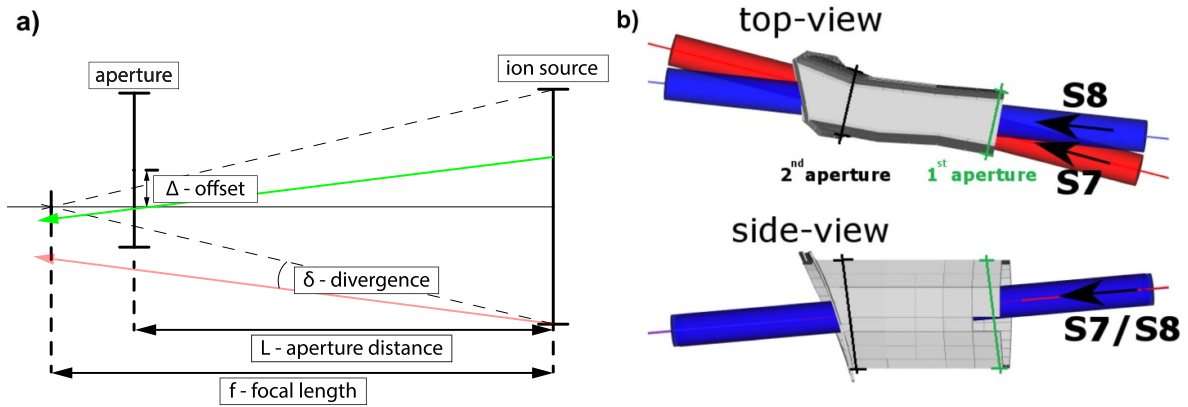


Figure 5. (a) Schematics of the neutral beam injection in a vertical cross-section used in FIDASIM. Markers are initialized at the ion-source position. (b) CAD drawing of the NBI lines (red and blue) with the beam duct (in grey) which provides the apertures marked with black and green lines.

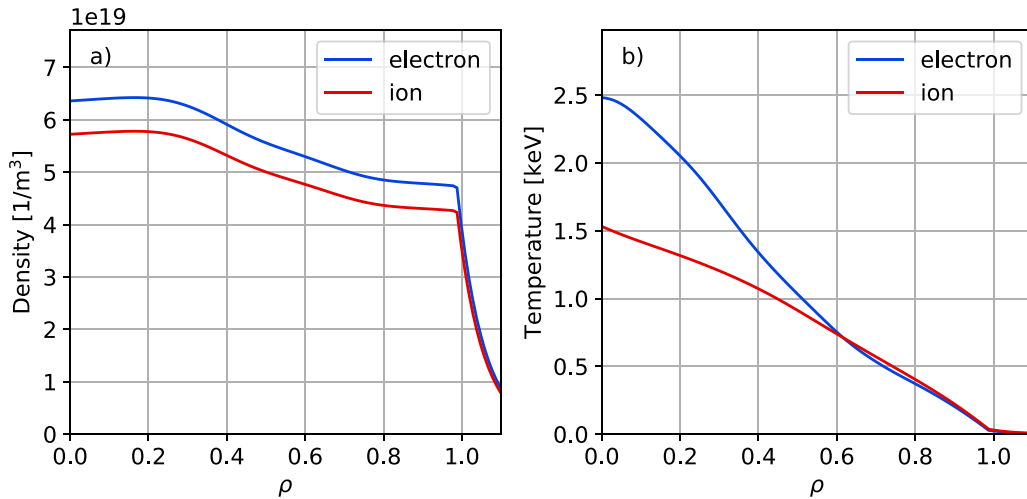


Figure 6. Kinetic profiles for discharge #20180823.037 at 4.6 s. (a) Density profiles, (b) temperature profiles. Radial electric field and toroidal rotation set to zero. The main impurity species is supposed to be carbon, as W7-X is a carbon wall device with assuming $Z_{\text{eff}} = 1.5$. Red curves are for ion- and blue curves are for electron parameters.

The edge kinetic profiles ($\rho > 1$) were neglected in the first calculations.

With these inputs, the beam emission spectra were predicted for all of the available lines of sight. Representative measured and predicted beam emission spectra of a LOS from the 45° view are shown in figure 7. The blue line represents the FIDASIM prediction of the beam emission and the black line shows the measured active spectrum after background subtraction and the removal of the fitted Bremsstrahlung emission. This is being performed by first taking the difference of two spectra, one 100 ms after, and a reference right before the NBIs are turned on. Then in the second step, any residual Bremsstrahlung is removed by fitting a constant background at the resulting difference spectra. As the measurement is absolutely calibrated, a direct comparison without scaling factor can be performed with simulations. We can see that the blue beam emission prediction is in good agreement with the measurement. Both the spectral shape and intensity are well reproduced by the FIDASIM prediction.

For further analysis, the FIDASIM-predicted total BES spectral shape (sum of all energy components) was fitted to the active measurement to obtain a measure of any global discrepancy between the experiment and simulation, as shown in figure 8. We can see in figure 8 that the FIDASIM-predicted total beam emission is in good agreement with the measurement, observing no significant trend over the whole plasma cross-section from the low-field side to the high-field side, staying within a $\pm 25\%$ error. This suggests that with the assumed profiles, the beam attenuation is calculated accurately by FIDASIM and that the 1.35 MW power per source to the torus is an accurate assumption. Thus, this method provides robust information on the NBI injection power to the torus value by scaling the BES intensity to best fit the measurements.

Though minor discrepancies are seen between the measurement and the simulation, which provide insight into the shape of the beam. For example, we can see in figure 8 that the scaling factor for port A21 (red dots) is systematically lower than one. Thus, the measured intensity is lower than

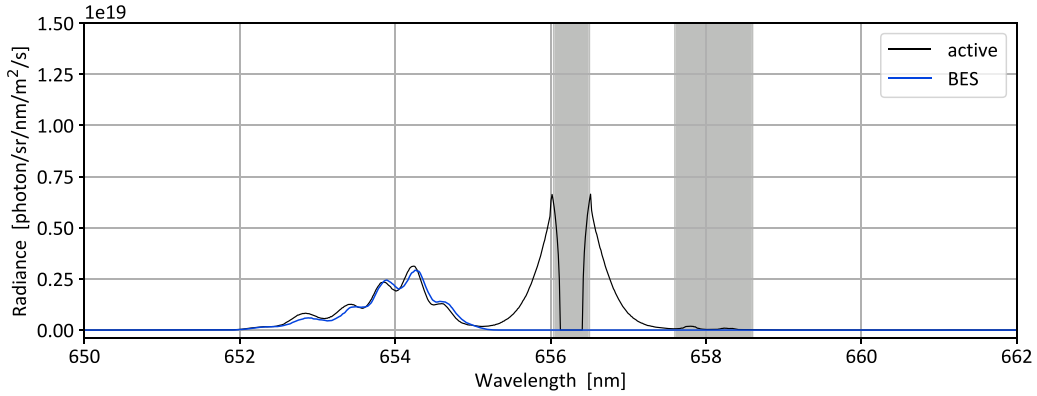


Figure 7. A typical active CXRS Balmer-alpha spectrum in discharge #20 180 823.037 for an M21 port observation (M21S7:12) at the low field side, with solid black line as the measured spectra, grey as the cold-Balmer alpha and carbon emission affected area, not included in the fitting, and blue as the FIDASIM predicted beam emission.

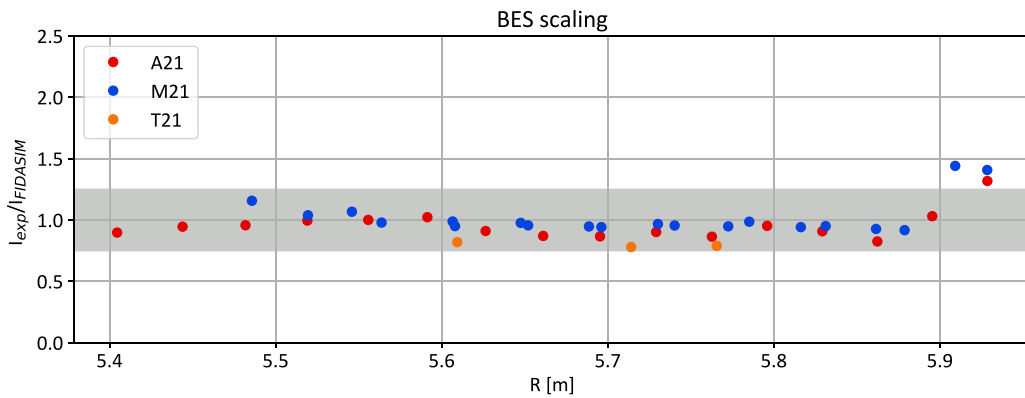
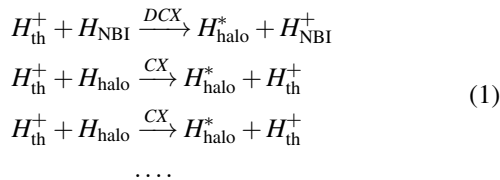


Figure 8. BES scaling factors obtained by fitting the FIDASIM predicted beam emission to the measured intensities. Different colors mark different observation ports.

what FIDASIM would suggest. As port A21 is looking toroidally at the beams it means that the vertical width of the beam could be wider, implying slightly higher divergence in this direction.

After predicting the beam emission, FIDASIM calculates the beam halo contribution. The halo emission originates from charge exchange reactions between beam neutrals and thermal ions (DCX), followed by a series of subsequent charge-exchange reactions (marked with ... in the equation) between thermal neutrals and thermal ions:



The spectral width, intensity, and Doppler-shift of the halo emission carries information on the main-ion temperature, density, and velocity respectively. A comparison for the predicted halo and beam neutral densities is shown in figure 9. The beam density of the $n=3$ state is on the same order of magnitude as that of the halo neutrals. Moreover, its spatial

distribution follows the beam shape such that the inferred main ion temperature and rotation will have a similar spatial localization as e.g. the carbon temperature from CXRS. Figure 10 shows a comparison of the predicted and measured halo emission for the reference experiment.

The predicted halo spectral shape matches well with the measured one which has a couple of implications. One is that the input ion temperature profile used, inferred from the CVI+ line width does explain the halo shape well, thus their spatial information must come from the same region. This is due to the high collisionality and moderate ion temperature of the reference plasma, which limits the size of the halo neutral population, overlapping with the CX carbon population. Second, it further confirms the reliability of the input beam parameters, and the beams' shape themselves.

Following a similar approach as for the investigation of the beam emission, figure 11 compares the ratio of the observed and FIDASIM-predicted halo emission total intensities.

The ratio is close to one in the core of the plasma ($5.5 \text{ m} < R < 5.9 \text{ m}$), while the measured halo emission becomes higher than the FIDASIM prediction (with a factor of 2) towards the edge region. Our hypothesis for this observation is, that passive thermal radiation contributes to the measurement,

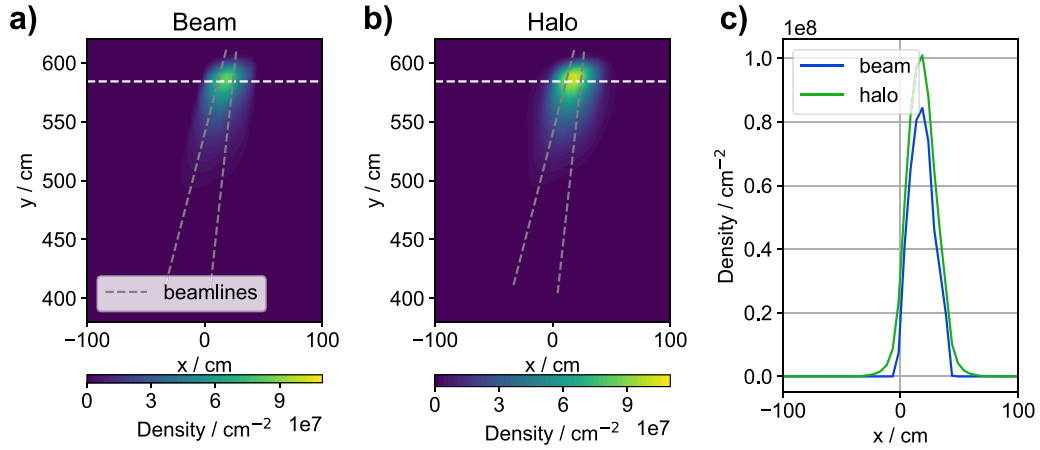


Figure 9. Neutral particle density of the $n = 3$ state as predicted by FIDASIM in discharge #20 180 823.037, integrated along the z -axis (i.e. top-down), (a) for the neutral beam density, (b) the halo density, (c) along the horizontal cut at $y = 585$ cm, marked with white dashed line. The beamlines are depicted with grey dashed lines.

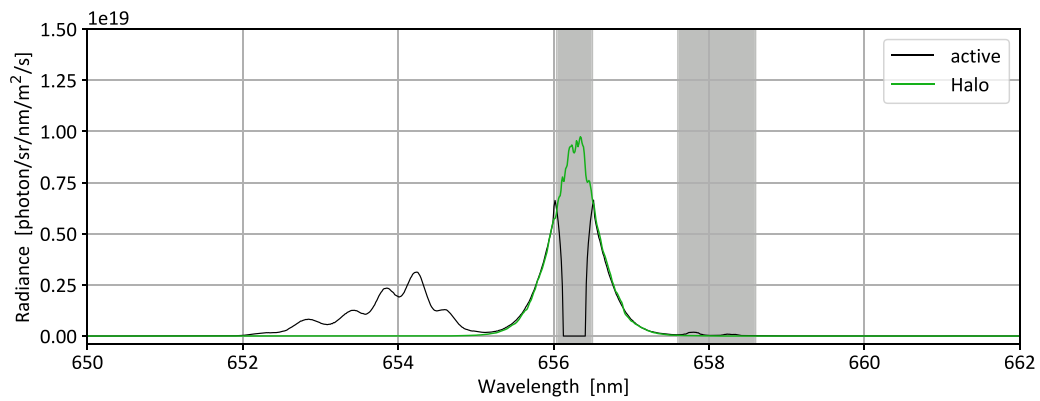


Figure 10. A typical measured active CXRS Balmer-alpha spectrum in discharge #20 180 823.037 with solid black line for an M21 port observation (M21S7:12) at the low field side. The cold-Balmer alpha and the carbon emission affected area is marked in grey and the FIDASIM predicted halo emission is plotted in green.

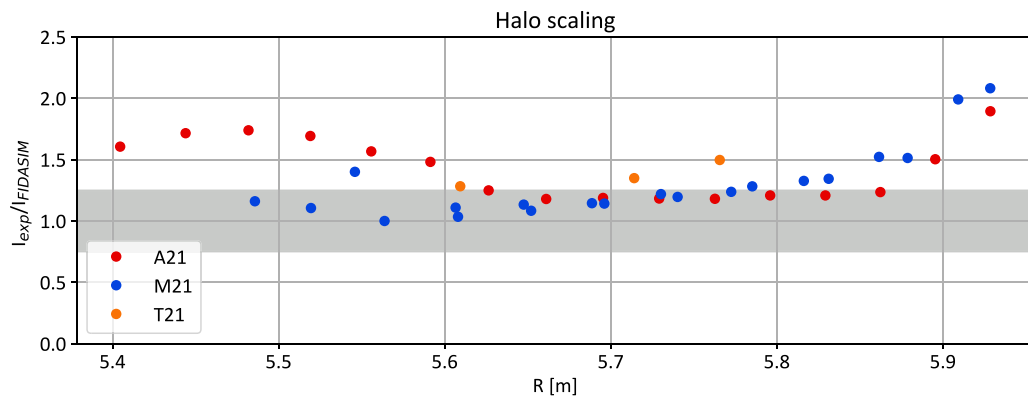


Figure 11. Beam halo scaling factors obtained from fitting the FIDASIM-predicted halo emission to the measured intensities. Different colors mark different ports for observation.

despite subtracting background radiation observed during phases without NBI. This is possible because NBI might not only generate fast neutrals but also act as a significant source of cold neutrals via wall sputtering. These cold neutrals can

have similar charge exchange reactions as in equation (1) and through numerous reactions can lead to further thermal halo emission in the edge region increasing the passive halo-like emission in the edge.

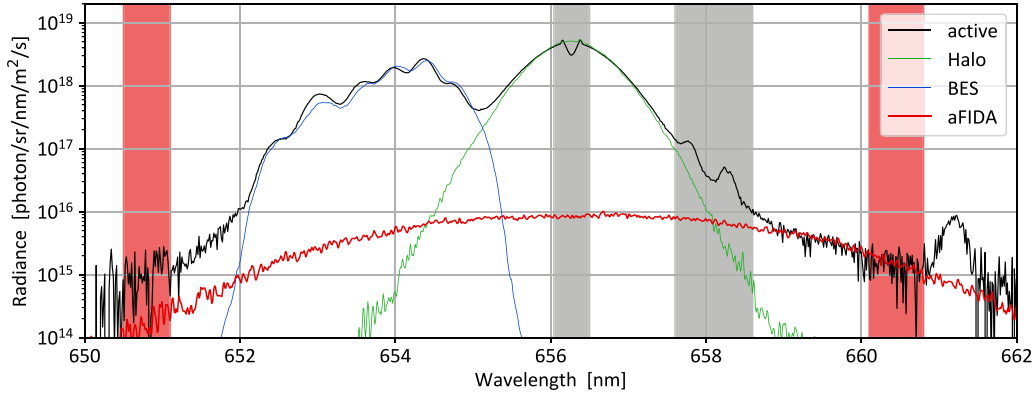


Figure 12. In black is shown a representative active CXRS Balmer-alpha spectrum, observed in discharge #20 180823.037 by an M21 port view (M21S7:16), located at the low field side. With grey, the cold Balmer-alpha and carbon emission affected area is marked. These regions are not included in any subsequent comparison. With red, the area used for fitting the predicted FIDA emission is marked. With red the FIDASIM predicted FIDA emission is plotted fitted to the measurement. Blue and green lines plot the previously fitted predicted BES and halo emission.

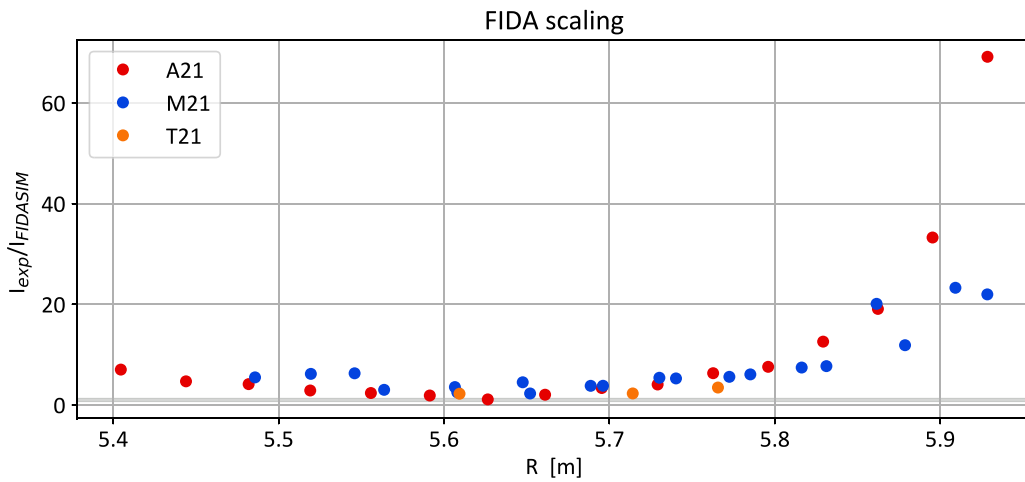


Figure 13. Active FIDA emission scaling factors obtained from matching the FIDASIM-predicted FIDA emission to the CXRS system measured absolute intensities. Different colors mark different ports for observation.

6. Confined fast-ions in W7-X and the observed spectra

With the beam and halo densities calculated, FIDASIM can calculate the FIDA emission based on an ASCOT predicted fast-ion distribution functions.

Figure 12 compares the measured active spectrum for a port M21-port observation (black) with the FIDASIM-predicted active FIDA emission (red) scaled to the measurement. The predicted active FIDA emission is fairly symmetrical around the non-Doppler-shifted line and matches well the shape of the measurement. Note here that the symmetrical shape of the emission is expected as the corresponding fast-ion distribution function, shown in figure 2, populates positive and negative pitch values. Apart from that, it should be noted that the blue-shifted side shows a larger discrepancy than the red-shifted counterpart. The scaling factors, required to best-fit the measured spectra of all available channels are given in figure 13.

Significant discrepancies are observed in the absolute intensities for all observation directions with an increasing ratio towards the edge of the plasma. Up to 60 times more radiation is observed close to the plasma edge than is predicted by FIDASIM. This suggests, once again, that the observed radiation originates from the edge region and is passive in nature, which has not yet been considered in our simulations. Partially because ASCOT predicted fast-ion distribution function only originates from the confined region, ignoring fast-particles getting ionized in the plasma edge ($\rho > 1.0$), partially because the cold, recycled neutrals are not yet included in the simulation. Apart from this scaling, several general statements can be made regarding the observed FIDA emission:

- The beam emission affected wavelength side has very limited use for FIDA analysis, as the FIDA signal is lower than the BES signal's uncertainty, it cannot be analyzed after its removal.

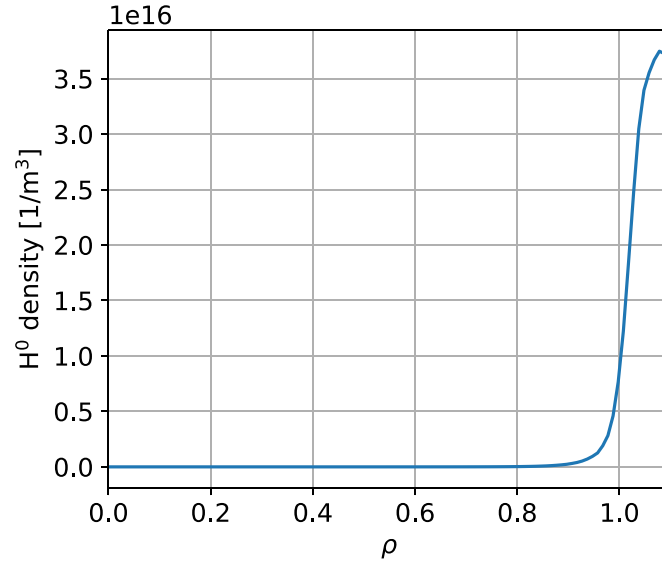


Figure 14. KN1D predicted recycled H^0 neutral density based on extrapolated kinetic profiles.

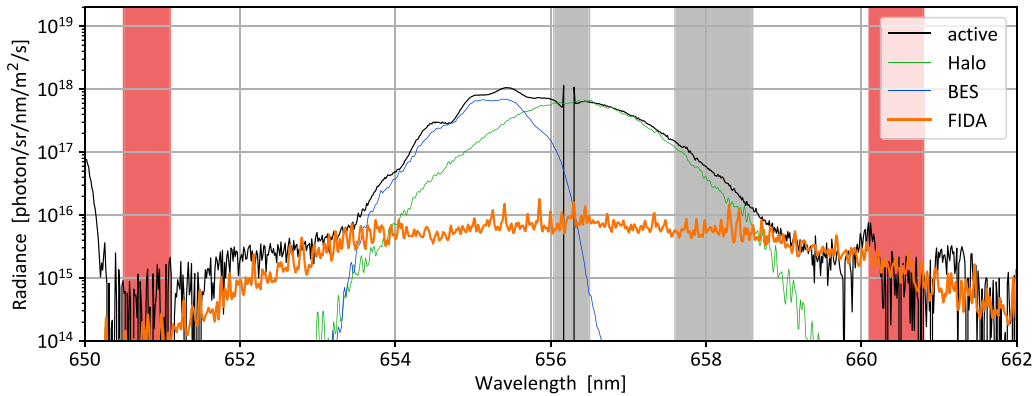


Figure 15. Typical measured Balmer-alpha spectrum with black, and with orange line the sum of the active FIDA and the scaled passive FIDA emission for an M21 view (M21S7:44) in the plasma core. Blue and green lines show the predicted BES and halo emission of the spectrum. With grey, the cold Balmer-alpha and carbon emission affected area is marked. These regions are not included in any subsequent comparison. With red, the area used for fitting the predicted FIDA emission is marked.

- Both sides of the spectrum are only usable for the FIDA analysis where the Doppler shifts of the beam emission are small.
- For the W7-X CXRS observation, this is in the plasma core for the M21 port, and in the plasma edge for A21 and T21 ports.
- Anywhere else, only one side of the spectrum can be utilized for detailed analysis.

6.1. Passive FIDA and halo emission modeling

Given the evident dominance of the passive FIDA signal, it is necessary to include the edge neutral density in order to correctly interpret the FIDA spectrum. To achieve this, the kinetic transport code for atomic and molecular hydrogen, KN1D [24] was used to predict a 1D neutral density profiles. For this, a couple of assumptions are made. Radial extensions of the kinetic profiles were made by 5 cm (which roughly corresponds to the SOL width [25]) and the wall temperature was set to 3 eV.

The predicted neutral profiles can be seen in figure 14. As all these parameters are not well defined our analysis focuses on the qualitative behavior of the neutral density and not at its absolute numbers.

With the neutral density, the passive FIDA emission can be simulated in FIDASIM, as previously done e.g. in [11]. The resulting emission is localized in the plasma edge and contributes most to lines of sight that are tangential to this region (the edge-localized LOS). Figure 15 shows an example FIDA spectrum where the passive contribution was included, and while keeping the active FIDA emission as predicted, the passive trace was scaled to best fit the spectra in the highlighted region. As can be seen, the spectral shape is very similar to that of the active spectrum seen before in figure 12.

Figure 16 shows results of the scaling analysis based on the predicted passive FIDA emission. Here, we assumed that the predicted active FIDA contribution is correct, and only the passive emission has been scaled to find the best match between measurement and simulation.

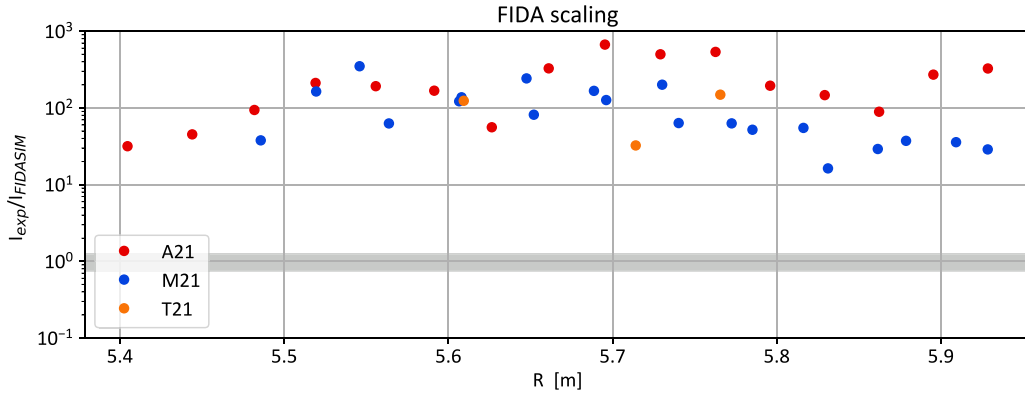


Figure 16. Passive FIDA emission scaling factors obtained from matching the FIDASIM predicted passive FIDA emission to the CXRS system measured absolute intensities minus the assumed active contribution. Different colors mark different ports for observation.

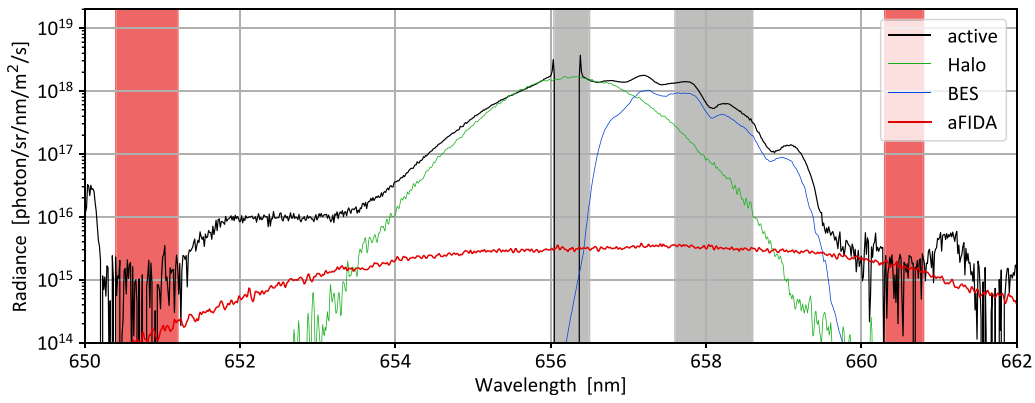


Figure 17. Experimental active CXRS spectrum measured in discharge #2180 823.037 for one of the T21 port observations (T21:14). With grey, the cold Balmer-alpha and carbon emission affected area is marked. These regions are not included in any subsequent comparison. With red, the area used for fitting the predicted FIDA emission is marked. The fixed active FIDA spectrum to the shaded area is plotted with a red line. Previously discussed halo and BES prediction is plotted with green and blue line. The shoulder like spectral feature can be observed in the 650–653 nm range.

We can see that the inclusion of the neutral density profile removes the majority of the spatial dependency of the intensity discrepancy, suggesting the remaining dependence of global scaling such as the edge neutral density. With the given neutral profile FIDASIM ends up underestimating the passive emission with an average of 103 ± 84 for M21, 101 ± 50 for T21 and 241 ± 182 for A21. In the case of the toroidal observation (A21 port), the estimated ratios are consistently higher as their integration length in the plasma is much higher than for the other two ports (M21 and T21), and as such we expect higher neutral densities. This observation promotes the assumption that W7-X edge density can reach fairly high values in the order of $O(10^{13}) \text{ cm}^{-3}$, but its detailed analysis is out of the scope of this paper.

6.2. Collision-less edge fast-ions and their FIDA spectra

An unexpected radiance plateau is observed only in spectra of the T21 views that is not explained by the modelling based on the ASCOT fast-ion distribution. Figure 17 shows an example case with a clear shoulder between 651.5–653.3 nm. The observed fall-off wavelength corresponds to the maximal Doppler-shift of the half energy (24 keV) component:

$$\Delta\lambda_{\max} = \lambda_0 \sqrt{\frac{2E_{\text{inj}}}{m_p c^2}} \approx 4.7 \text{ nm}. \quad (2)$$

To help explain this observation a local fast-ion distribution function was needed in the plasma edge, in front of the T21 port. Full-orbit particle tracing was applied in the plasma edge, to predict the local pitch and energy distribution of fast ions particles born there. Using FIDASIM we predicted the birth location of fast-ions, from where they were traced using Boris integration scheme, including the slowing down as in [26]. It was found that a significant portion of these fast-particles (initialized between $0.9 < \rho < 1.1$) end up within 3 cm of the T21 port lines of sight in less than a μs . Compared to this, the local collision time is three orders of magnitude larger, in the 10 ms range. Assuming a local 10^{13} cm^{-3} neutral density, the charge-exchange time is in the same μs order. At this minimal distance, their pitch distribution was calculated, which is visualized in figure 18. As the full energy component particles have deeper penetration depth (smaller ionization rate in the SOL region), the main contributors of these edge-born fast-ions are the half and third energy component ones. Moreover, it should be noted that there is no significant difference in the pitch distribution between different energies as the pitch

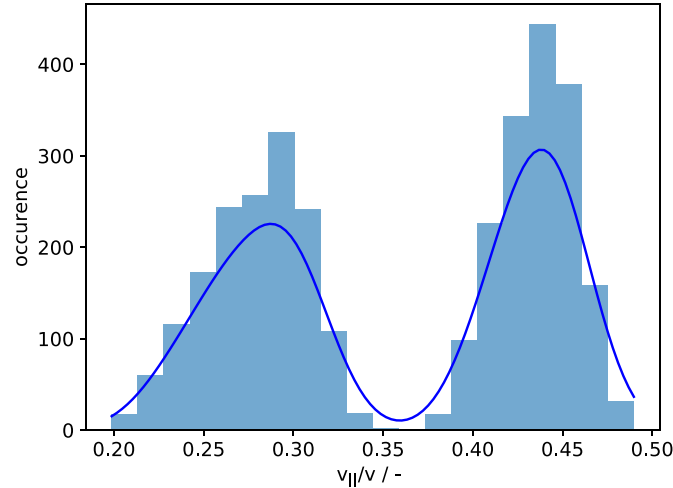


Figure 18. Pitch distribution of fast particles at their minimum distance from the T21 port observation. Bars show the binning of the tracked particles, continuous line shows the fitted kernel density function. The two distinguishable peaks are corresponding to the S7 and S8 slightly different injection respectively.

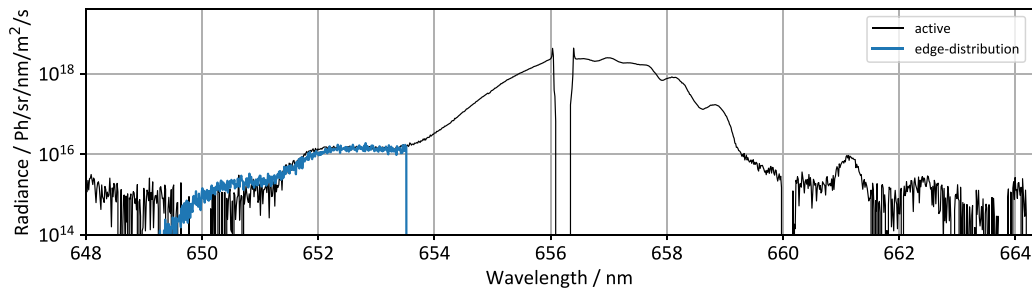


Figure 19. Passive FIDA spectrum with the assumed collision-less fast-ion pitch distribution as predicted by FIDASIM scaled to the measurement.

is the characteristic of the source itself. Using this as input for FIDASIM, passive FIDA spectra have been predicted, as e.g. shown in figure 19.

We can see that the predicted light coincides extremely well with the observation, proving that its source is indeed collision-less particles born in the plasma edge, ending up in the proximity of the observation, while having high neutral densities simultaneously. It should be noted that this feature has not been contained in the passive FIDA spectra using ASCOT distribution functions since ASCOT neglects the ionization of fast ions in the SOL region. This shows that the careful inclusion of the SOL beam attenuation, charge-exchange processes, and fast ion birth in ASCOT would be needed for a more complete modelling of W7-X plasmas.

7. Conclusions

FIDASIM has been adapted successfully at Wendelstein 7-X, exploiting the code's novel full 3D modeling capabilities. The device's NBI geometry has been implemented, including beam scraping elements and the beam attenuation model of FIDASIM has been validated successfully against beam emission measurements and calorimetry. Furthermore, the halo neutral density and its emission were predicted, showing

good agreement with measurements allowing for some contribution due to edge recycling neutrals. These steps provide confirmation of the proper, state-resolved modelling of active neutral hydrogen sources (beam and halo neutrals) and their corresponding spectral contribution to the Balmer-alpha spectrum. However, it was initially not possible to find a good match between the active FIDA emission and the FIDASIM prediction, in particular for lines of sight close to the plasma edge where the measured FIDA signals are more than ten times larger than what is expected based on ASCOT-predicted fast-ion distribution functions. This leads to the conclusion that the observed light in the plasma edge is dominantly passive, coming from the charge-exchange recombination of fast-ions and recycled cold neutrals. For heuristic modelling of this, KN1D provided 1D neutral profiles and a full-orbit modelling code has been applied to predict the passive FIDA radiation from the edge. With this approach, an excellent agreement has been observed between the observed spectral shapes of the FIDA emission and the measurements. This shows that proper modelling of the scrape-off layer plasma is critical to interpret the FIDA emission. Moreover, it opens the possibility that passive FIDA measurements could be used, with the aid of FIDASIM, to probe the SOL fast-ion distribution function in future experiments—given the neutral density is sufficiently well known. Finally, it needs to be noted that the installation

and commissioning of further NBI sources, which do not cross the lines of sight of the CXRS system, will enable the experimental separation of the active and passive FIDA emissions, allowing us to further investigate their properties, separately.

Acknowledgments

This work has been carried out within the framework of the EUROfusion consortium and has received funding from the Euratom research and training programme 2014–2018 and 2019–2020 under Grant Agreement Number 633053. The views and opinions expressed herein do not necessarily reflect those of the European Commission.

ORCID iDs

Peter Zs. Poloskei  <https://orcid.org/0000-0001-7781-5599>
 B. Geiger  <https://orcid.org/0000-0001-8706-1874>
 A. Jansen van Vuuren  <https://orcid.org/0000-0003-1732-3642>
 S. Äkäslompolo  <https://orcid.org/0000-0002-9554-5147>
 O.P. Ford  <https://orcid.org/0000-0002-5646-4758>
 D. Hartmann  <https://orcid.org/0000-0002-3511-6500>

References

- [1] Heidbrink W.W., Luo Y., Burrell K.H., Harvey R.W., Pinsker R.I. and Ruskov E. 2007 Measurements of fast-ion acceleration at cyclotron harmonics using Balmer-alpha spectroscopy *Plasma Phys. Control. Fusion* **49** 1457
- [2] Adamov M.R.G., Obradovic B.M., Kuraica M.M. and Konjevic N. 2003 Doppler spectroscopy of hydrogen and deuterium Balmer alpha line in an abnormal glow discharge *IEEE Trans. Plasma Sci.* **31** 444–54
- [3] Heidbrink W.W., Burrell K.H., Luo Y., Pablant N.A. and Ruskov E. 2004 Hydrogenic fast-ion diagnostic using Balmer-alpha light *Plasma Phys. Control. Fusion* **46** 1855
- [4] Von Hellermann M.G., Mandl W., Summers H.P., Weisen H., Boileau A., Morgan P.D., Morsi H., Koenig R., Stamp M.F. and Wolf R. 1990 Visible charge exchange spectroscopy at jet *Rev. Sci. Instrum.* **61** 3479–86
- [5] Kukushkin A.B., Neverov V.S., Kadomtsev M.B., Kotov V., Kukushkin A.S., Levashova M.G., Lisgo S.W., Lisitsa V.S., Shurygin V.A. and Alekseev A.G. 2014 Parameterization of Balmer-alpha asymmetric line shape in tokamak SOL plasmas *J. Phys.: Conf. Ser.* **548** 012012
- [6] Von Hellermann M., de Bock M., Marchuk O., Reiter D., Serov S. and Walsh M. 2019 Simulation of spectra code (SOS) for ITER active beam spectroscopy *Atoms* **7** 30
- [7] Heidbrink W.W., Liu D., Luo Y., Ruskov E. and Geiger B. 2011 A code that simulates fast-ion $D\alpha$ and neutral particle measurements *Commun. Comput. Phys.* **10** 716–41
- [8] Geiger B. et al 2020 Progress in modelling fast-ion D-alpha spectra and neutral particle analyzer fluxes using FIDASIM *Plasma Phys. Control. Fusion* **62** 105008
- [9] Geiger B., Garcia-Munoz M., Heidbrink W.W., McDermott R.M., Tardini G., Dux R., Fischer R. and Igochine V. 2011 Fast-ion D-alpha measurements at ASDEX upgrade *Plasma Phys. Control. Fusion* **53** 065010
- [10] Luo Y., Heidbrink W.W., Burrell K.H., Kaplan D.H. and Gohil P. 2007 Measurement of the $D\alpha$ spectrum produced by fast ions in DIII-D *Rev. Sci. Instrum.* **78** 033505
- [11] Geiger B., Karpushov A., Duval B., Marini C., Testa D. and DiCampli R. 2017 Study of the fast-ion distribution function in the TCV tokamak based on FIDA spectroscopy and the TRANSP code *Plasma Phys. Control. Fusion* **59** 115002
- [12] Isler R.C. 1994 An overview of charge-exchange spectroscopy as a plasma diagnostic *Plasma Phys. Control. Fusion* **36** 171
- [13] Grierson B.A., Burrell K.H., Chrystal C., Groebner R.J., Haskey S.R. and Kaplan D.H. 2016 High resolution main-ion charge exchange spectroscopy in the DIII-D H-mode pedestal *Rev. Sci. Instrum.* **87** 11E545
- [14] Fujiwara Y. et al (LHD Experiment Group) 2019 Evaluation of an energetic particle profile using a tangential-FIDA diagnostic in the large helical device *Plasma Fusion Res.* **14** 3402129
- [15] Klinger T. et al 2019 Overview of first Wendelstein 7-X high-performance operation *Nucl. Fusion* **59** 112004
- [16] Spanier A. et al 2021 Performance of the first neutral beam injector at the Wendelstein 7-X stellarator *Fusion Eng. Des.* **163** 112115
- [17] McNeely P. et al 2020 Commissioning and initial operation of the W7-X neutral beam injection heating system *Fusion Eng. Des.* **161** 111997
- [18] Wolf R.C. et al 2019 Performance of Wendelstein 7-X stellarator plasmas during the first divertor operation phase *Phys. Plasmas* **26** 082504
- [19] Ford O.P. et al 2020 Charge exchange recombination spectroscopy at Wendelstein 7-X *Rev. Sci. Instrum.* **91** 023507
- [20] Grahl M., Svensson J., Werner A., Andreeva T., Bozhenkov S., Drevlak M., Geiger J., Krychowiak M. and Turkin Y. 2018 Web services for 3D MHD equilibrium data at Wendelstein 7-X *IEEE Trans. Plasma Sci.* **46** 1114–9
- [21] Äkäslompolo S. et al 2019 Validating fast-ion wall-load IR analysis-methods against W7-X NBI empty-torus experiment *J. Instrum.* **14** 07018
- [22] Weiland M., Geiger B., Jacobsen A.S., Reich M., Salewski M. and Odstrčil T. 2016 Enhancement of the FIDA diagnostic at ASDEX Upgrade for velocity space tomography *Plasma Phys. Control. Fusion* **58** 025012
- [23] Geiger J., Beidler C.D., Feng Y., Maaßberg H., Marushchenko N.B. and Turkin Y. 2014 Physics in the magnetic configuration space of W7-X *Plasma Phys. Control. Fusion* **57** 014004
- [24] Bombard B. 2001 *KNID: A 1-D space kinetic, 2-D velocity, transport algorithm for atomic molecular hydrogen in an ionizing plasma* Research Report PSFC-RR-01-3 Massachusetts Institute of Technology
- [25] Killer C. et al 2019 Characterization of the W7-X scrape-off layer using reciprocating probes *Nucl. Fusion* **59** 086013
- [26] Weiland M. et al (Eurofusion MST1 Team) 2018 RABBIT: real-time simulation of the nbi fast-ion distribution *Nucl. Fusion* **58** 082032